Applied Plasma Spectroscopy: Laser-Fusion Experiments

Introduction

The remarkable progress of laser-fusion experiments [i.e., inertial confinement fusion (ICF) driven by high-intensity laser beams] has been charted with x-ray spectroscopy. Hans Griem, considered the father of plasma spectroscopy, provided an excellent foundation for this research.[1] Inertial confinement fusion occurs when a spherical-shell target containing thermonuclear fuel [i.e., deuterium and tritium (DT)] is imploded to produce energy gain.[2,3] The implosion is driven by the ablation of material from the outer shell surface with intense laser beams (direct drive)[2] or with x rays produced in a high-Z enclosure or hohlraum (indirect drive).[3] Both of these schemes rely on the solid-state Nd:glass laser invented by Elias Snitzer in 1961.[4] High-power Nd:glass laser beams were developed at LLE and Lawrence Livermore National Laboratory (LLNL) in the 1960s and 1970s, as well as in France, Japan, and Russia.[5] Historically, indirect-drive[3] ICF was pursued at LLNL, while direct-drive[2] implosions were the main focus of the LLE research program.

Four areas of x-ray spectroscopy for laser-fusion experiments are highlighted in this article: K_α emission spectroscopy to diagnose target preheat by suprathermal electrons,[6–10] Stark-broadened K-shell emissions of mid-Z elements to diagnose compressed densities and temperatures of implosion cores,[11–13] K- and L-shell absorption spectroscopy to diagnose the relatively cold imploding shell that does not emit x rays,[14–16] and multispectral monochromatic imaging of implosions to diagnose core temperature and density profiles.[17–20] The original x-ray-spectroscopy experiments in these areas will be discussed and compared to current state-of-the-art measurements. This article concentrates on direct-drive ICF[2] since laser ablation was used to create the high-energy-density plasmas probed with x-ray spectroscopy in the highlighted research. LLE Senior Scientist B. Yaakobi pioneered many of the x-ray-spectroscopy experiments in laser-fusion research.[6,8,9,11,12,14,18]

Over the last three decades, increasing amounts of energy have been delivered to target with multibeam Nd:glass laser systems.[5] At LLE, the four-beam DELTA laser,[21] operating at 1ω with 10 J in a 40-ps pulse, evolved into the OMEGA Laser System,[22] which consists of a 60-beam, 3ω, 30-kJ compression laser and the high-energy petawatt OMEGA EP laser.[23] The uniformity of direct-drive implosions steadily improved with scientific advancements in laser technology and target physics. Laser-irradiation nonuniformity levels approaching 1%–2% rms[24] were achieved using phase plates,[25] two-dimensional (2-D) smoothing by spectral dispersion (SSD),[26] polarization smoothing (PS),[27] and a large number of symmetrically arranged laser beams. The hydrodynamic efficiency of laser ablation was significantly improved by frequency tripling the fundamental 1ω laser wavelength.[28] The size of the gas-filled spherical-shell implosion targets increased more than an order of magnitude to ~1 mm. X-ray streak cameras[29] were developed to record time-resolved x-ray spectra. Significant theoretical advances in spectral line-shape calculations were made,[30–35] beginning with the realization by H. Griem that the distribution of electric microfields of the ions and electrons led to Stark broadening of spectral line shapes in plasmas.[1] Increases in computational power kept pace with Moore's law[36] and made it feasible to more accurately calculate complex spectra.[30–35] Progress on all these fronts paved the way to highly reproducible x-ray spectroscopic results for laser-fusion experiments, which complemented measurements of charged-particle spectroscopy and neutronics.[2,3] The next step of thermonuclear ignition on the soon-to-be-completed 192-beam, 1.8-MJ National Ignition Facility (NIF) laser system[37] at LLNL will greatly benefit from these results.

The following sections present a brief introduction to laser-fusion research, describe the plasma spectroscopy applications in laser-fusion experiments, and summarize our conclusions.

Inertial Confinement Fusion

Over the last three decades, x-ray spectroscopy has recorded the remarkable progress made in inertial confinement fusion. Hot-spot ignition involves the implosion of a thin-shell spherical target containing a cryogenic-DT layer.[2,3] For direct-drive ICF, a 3ω shaped laser pulse designed to achieve nearly isentropic compression initially irradiates the target with a low-intensity

foot (10^{13} to 10^{14} W/cm^2), followed by a high-intensity main drive (10^{15} W/cm^2) (Refs. 2 and 3). The laser irradiation breaks down the target surface and forms a coronal plasma. The laser energy is absorbed in the corona via inverse bremsstrahlung[2,3] and transported to the ablation surface via electron thermal conduction.[2,3] The ablated shell mass forms a coronal plasma that surrounds the target and accelerates the shell or pusher inward via the rocket effect.[2,3] The implosion can be divided into the following four stages (as illustrated in Fig. 118.1): shock propagation, acceleration phase, deceleration phase, and peak compression.[2,3]

Laser ablation launches hydrodynamic waves through the fuel layer and sets the target on the desired shell adiabat during the foot pulse. Shock heating is the main heating mechanism of the shell in an ablatively driven implosion.[2,3] The shell adiabat is defined as the ratio of shell pressure to the Fermi-degenerate pressure.[2,3] High compressibility requires that the DT fuel remains close to Fermi degenerate throughout the implosion. The dense, nearly Fermi degenerate matter or warm dense matter created by the shock waves is diagnosed with x-ray absorption spectroscopy using surrogate-planar, plastic-tamped Al targets.[15,16]

As the laser intensity rises during the main drive and the shock wave breaks out of the rear surface of the shell, the target begins to accelerate. Modulations at the ablation surface caused by mass perturbations and laser-irradiation nonuniformities are amplified by Rayleigh–Taylor (RT) hydrodynamic instability and feed through to the inner shell surface.[2,3] The corona evolves into a long-scale-length plasma and becomes susceptible to two-plasmon-decay (TPD) instability, which occurs near quarter-critical density when the phase-matching conditions are satisfied for the laser light to decay into two electron-plasma waves or plasmons.[38,39] Wave–particle interactions (e.g., Landau damping, trapping, and wave breaking) can generate suprathermal electrons with energies greater than 50 keV (Ref. 39). These hot electrons can preheat the fuel and adversely affect the target compressibility.[2,3] K_α emission spectroscopy of targets with buried mid-Z tracer layers is used to infer levels of target preheat.[6–9]

When the higher-density shell converges toward the target center and is decelerated by the lower-density fuel, a hot spot forms.[2,3] The hot dense matter created in the implosion core is diagnosed with x-ray emission spectroscopy.[11–13] The cold dense shell surrounding the hot spot is diagnosed with x-ray absorption spectroscopy.[14] The RT instability on the inner shell surface, seeded by feedthrough of nonuniformities from the ablation surface and by mass modulations on the inner surface, causes hydrodynamic mixing of the cold dense shell plasma with the hot-spot plasma. The radiative properties of hot dense matter with pressures of ~10 Gbar and the implosion dynamics of an Ar-doped-deuterium-gas–filled plastic-shell target are illustrated using the Stark-broadened spectral line shapes of Ar K-shell emission.[13] Levels of mixing of the plas-

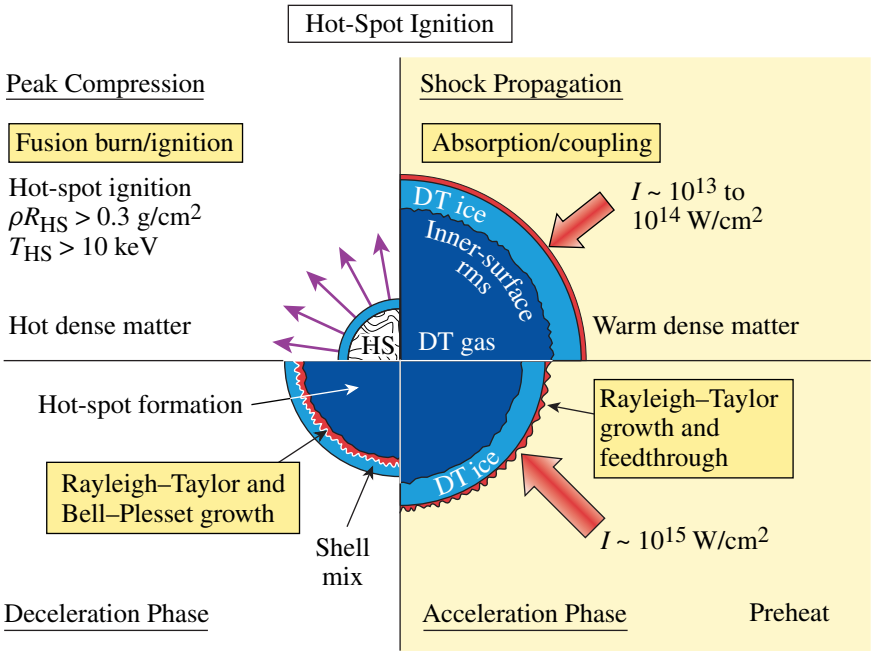

E14874bJR

Figure 118.1
Schematic illustrating the four stages—shock propagation, acceleration phase, deceleration phase, and peak compression—of a direct-drive implosion for hot-spot ignition.

tic shell with the deuterium fuel are estimated by combining x-ray spectroscopic results with fuel densities inferred from charged-particle spectroscopy.[40,41] The electron temperature and density profiles of the hot spot are inferred from multiple monochromatic x-ray imaging.[20]

Compression by the cold dense shell causes the pressure and DT fusion reaction rate of the hot spot to increase. It is predicted that the α-particle fusion products will deposit sufficient energy in the hot spot to launch a thermonuclear burn wave out through the cold dense fuel in the shell just prior to peak compression, when the areal density of the hot spot exceeds 0.3 g/cm^2 and the hot-spot temperature reaches 10 keV (Refs. 2 and 3). Energy gain with hot-spot ignition depends on the implosion velocity of the shell V_{imp}, the shell areal density ρR_{shell} at the time of burn, and the in-flight shell adiabat.[2,3,42–44] A complementary approach to hot-spot ignition is fast ignition, which uses a high-energy petawatt laser to generate a beam of electrons or ions to heat a compressed mass to thermonuclear conditions.[45] Fast ignition reduces the drive uniformity requirements of the compression laser.

Laser-Fusion Experiments

The four areas of x-ray spectroscopy for laser-fusion experiments are presented in the order in which the seminal papers were published to emphasize the pursuit of the research. More-sophisticated target-physics experiments have accompanied the advances in laser-driver development. K_α emission spectroscopy used to diagnose target preheat by suprathermal electrons was reported first,[6] followed by measurements of Stark-broadened K-shell emissions of mid-Z elements to diagnose compressed densities and temperatures of implosion cores.[11] These experiments were performed on the four-beam DELTA Laser System.[21] K- and L-shell absorption spectroscopy used to diagnose the relatively cold imploding shell on DELTA[14] was reported several years later, along with backlighting using multifrequency x rays to diagnose the temperature and areal density of the implosion core on the two-beam GEKKO II Laser System.[17] The concept of combining a pinhole aperture with a Bragg crystal spectrometer to achieve multiple monochromatic x-ray images was extended to hundreds of pinholes nearly two decades later on the 60-beam OMEGA Laser System.[18] The original x-ray-spectroscopy experiments in these areas are discussed in this section and compared to current state-of-the-art measurements.

1. K_α Emission Spectroscopy

K_α emission spectroscopy was first used by Yaakobi *et al.*[6] to infer preheat by fast electrons in laser-fusion experiments. The four-beam, 1ω, 0.8-TW DELTA Laser System irradiated thin (~1-μm-thick) 90-μm-diam spherical glass shells filled with 10 atm of Ne gas with peak intensities of 2 to 3 × 10^{15} W/cm^2 as shown in Fig. 118.2(a). The 1ω laser irradiation generates suprathermal electrons via resonance absorption with energies of ~10 keV (Ref. 39). Such energetic electrons deposit their energy throughout the target shown in Fig. 118.2(a), resulting in K_α emission from the Ne-gas fill. In contrast to the ablatively driven implosion where the shock wave is the dominant heating mechanism of the shell, the rapid heating of the thin glass shell by suprathermal electrons and x-ray radiation from the

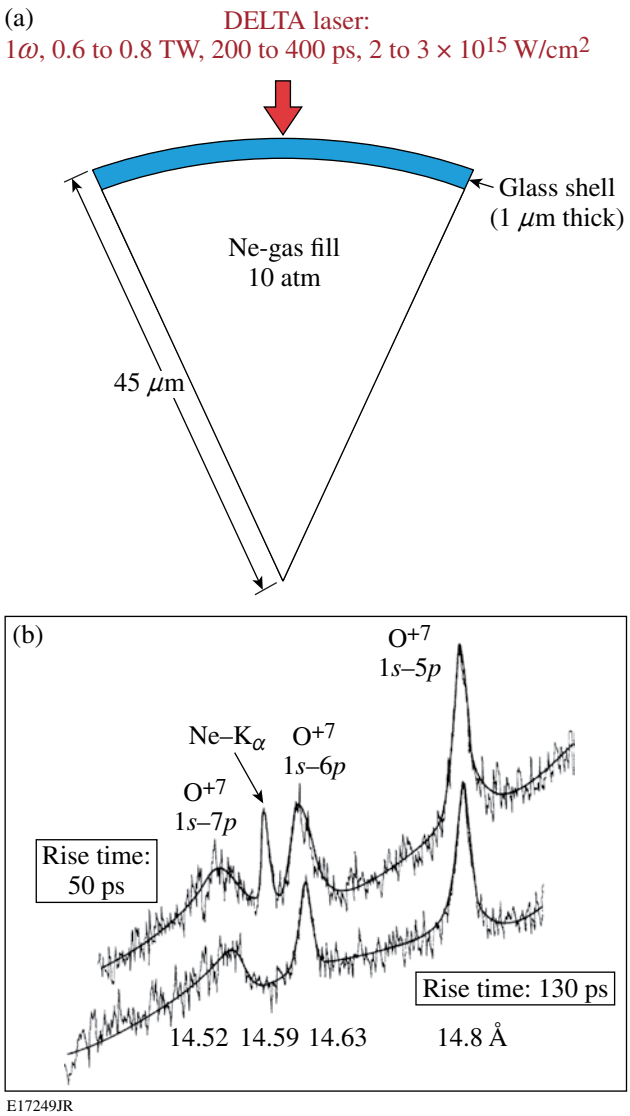

Figure 118.2
(a) Schematic of a direct-drive target, consisting of a thin glass shell filled with Ne gas, used in preheat experiments on the DELTA Laser System. (b) Measured, time-integrated x-ray spectrum showing Ne K_α emission.

corona causes the entire shell to explode. This type of implosion is called an exploding pusher: roughly half of the shell mass explodes outward and the remaining half inward, driving the implosion.[46] The number of fast electrons was estimated from the calibrated time-integrated x-ray spectrum of the Ne K_α emission shown in the upper trace in Fig. 118.2(b). This experiment did not shield the Ne gas from the coronal x-ray emission so the magnitude of the photopumping of the Ne K_α emission was estimated. Subsequent work by Hares *et al*. eliminated the effects of photopumping and saturation of K_α emission caused by ionization.[7] Multilayer planar targets composed of different elements, as shown in Fig. 118.3(a), shielded the K_α fluorescer from being photopumped by the x-ray radiation of the corona.[7] These planar targets were irradiated with conditions similar to the spherical targets in Yaakobi's experiment. The K_α emission characteristic of each layer, shown in Fig. 118.3(b), discriminates among the various excitation mechanisms and provides a higher-fidelity inference of the fast electrons.

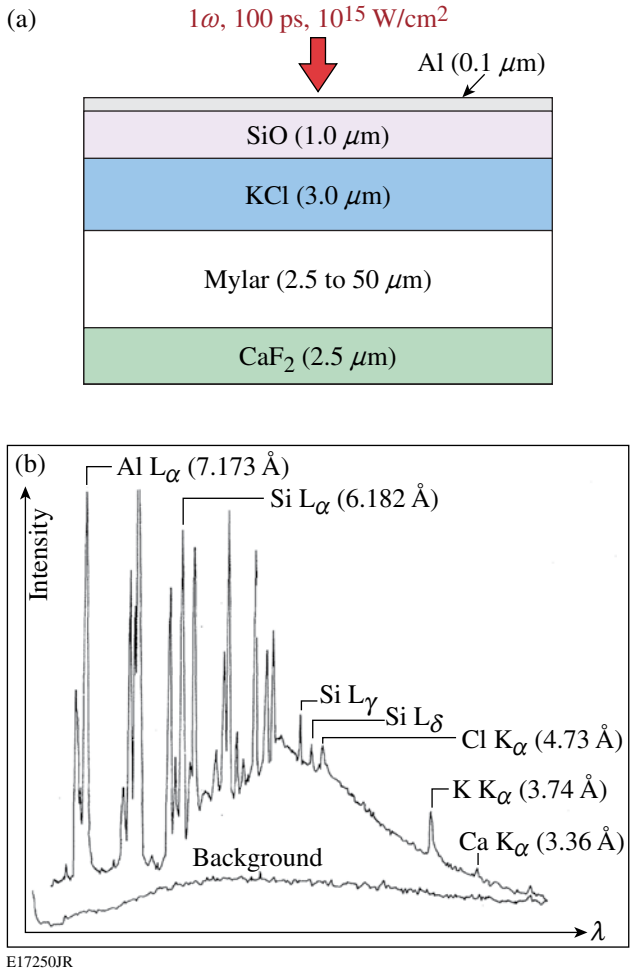

Figure 118.3
(a) Schematic of planar multilayer target used for preheat experiments and designed to discriminate between excitation mechanisms of photopumping from the coronal x-ray emission and fast electrons. (b) Measured, time-integrated x-ray spectrum showing K_α emission characteristic of each tracer layer.

Current state-of-the-art preheat measurements carried out on OMEGA for plastic-shell[8] and cryogenic-deuterium-shell[9] implosion targets rely on K_α emission spectroscopy to calibrate hard x-ray diagnostics[47] used to infer preheat. Similar experiments are also performed for fast ignition;[10,45] however, in stark contrast to hot-spot ignition, fast ignition must maximize the conversion of laser energy into hot electrons. Laser-to-hot-electron conversion-efficiency measurements were performed on the Nova 1ω, 400-J, 0.5- to 20-ps petawatt laser.[10] Planar Al/Mo/CH targets were irradiated with focused intensities of 0.02 to 3.0×10^{20} W/cm^2, and conversion efficiencies of ~50% were inferred at the highest intensity using Mo $K_{\alpha,\beta}$ spectroscopy.

2. X-Ray Emission Spectroscopy

The Stark-broadened spectral line shapes of the K-shell emission from mid-Z tracer elements provide a time-resolved measure of the electron temperature and density of the imploding core. Hans Griem showed that the distribution of the electric microfields of the ions and electrons led to Stark broadening of spectral line shapes in plasmas.[1] His former graduate student, Chuck Hooper, extended spectral-line-shape calculations to mid-Z elements with his research group at the University of Florida at Gainesville.[30] The hot dense matter created by spherical compression was diagnosed first by Yaakobi using the Stark-broadened K-shell emission of mid-Z tracer elements in the gas fill of spherical-shell implosion targets.[11] The four-beam, 1ω, 0.2-TW, 40-ps DELTA Laser System irradiated thin (~1-μm-thick), ~70-μm-diam spherical glass shells filled with 2 to 8.6 atm of Ne gas, as shown in Fig. 118.4(a). Compressed densities in the cores of exploding pusher implosions were diagnosed using Stark broadening of Ne K-shell emissions. As shown in Fig. 118.4(b), an electron density of 7×10^{22} cm^{-3} was inferred from Stark broadening of Ne Lyman-γ emission, which was calculated by Chuck Hooper's atomic physics group.[30] Yaakobi extended this work to the ZETA Laser System,[12] which was the first six-beam laser system of the 24-beam OMEGA Laser System.[48] The six-beam, 1ω, 100-J, 50-ps ZETA Laser System irradiated thin (~0.5- to 2-μm-thick) spherical glass shells with (1.5- to 4.2-μm-thick) plastic ablators ~50 μm in diameter and filled with 3 to 16 atm of Ar gas, as shown in Fig. 118.5(a). Increasing the thickness of the shell with the CH ablator changes the implosion from an exploding pusher[46] to an ablatively driven implosion. The compressed mass density and temperature were inferred from the He_β Stark-broadened, Ar K-shell spectral line shapes shown in Fig. 118.5(b). Again, the

predicted spectral line shapes were calculated by Hooper.[30] This x-ray spectroscopic observation demonstrated that symmetric illumination (six beam) with an ablatively driven implosion leads to high-volumetric convergence (>1000) (Ref. 12).

Laser-fusion experiments worldwide use Stark-broadened spectral line shapes to diagnose implosions.[11–13,30,31,34,49–54] The development of more-sophisticated codes to calculate the Stark-broadened spectral line shapes accompanied these experimental advances.[30–35] Hooper's atomic physics group developed the Multi-Electron Radiator Line Shape (MERL) code,[32] which uses the adjustable parameter exponential approximation (APEX)[33] for ion-microfield calculation, and a quantum-mechanical relaxation approximation for electron broadening.[34] The asymmetry of the Stark-broadened Ar K-shell emission was studied.[31] Kilkenny *et al.* performed a more-rigorous analysis of the spectral line shapes measured on a two-beam Ne:glass laser at the Rutherford Laboratory Cen-

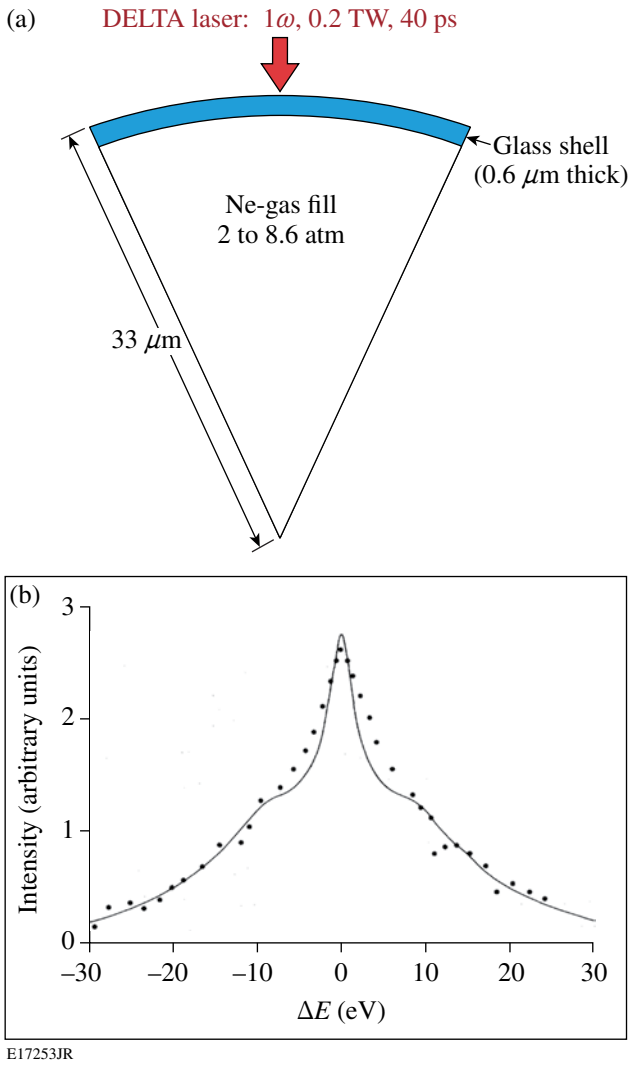

Figure 118.4
(a) Schematic of a direct-drive target, consisting of a thin glass shell filled with Ne gas, used in implosion compression experiments on the DELTA Laser System. (b) Measured, time-integrated x-ray spectrum of the Stark-broadened Ne Ly_γ emission (solid circles), compared to the predicted[30] spectral line shape (solid curve).

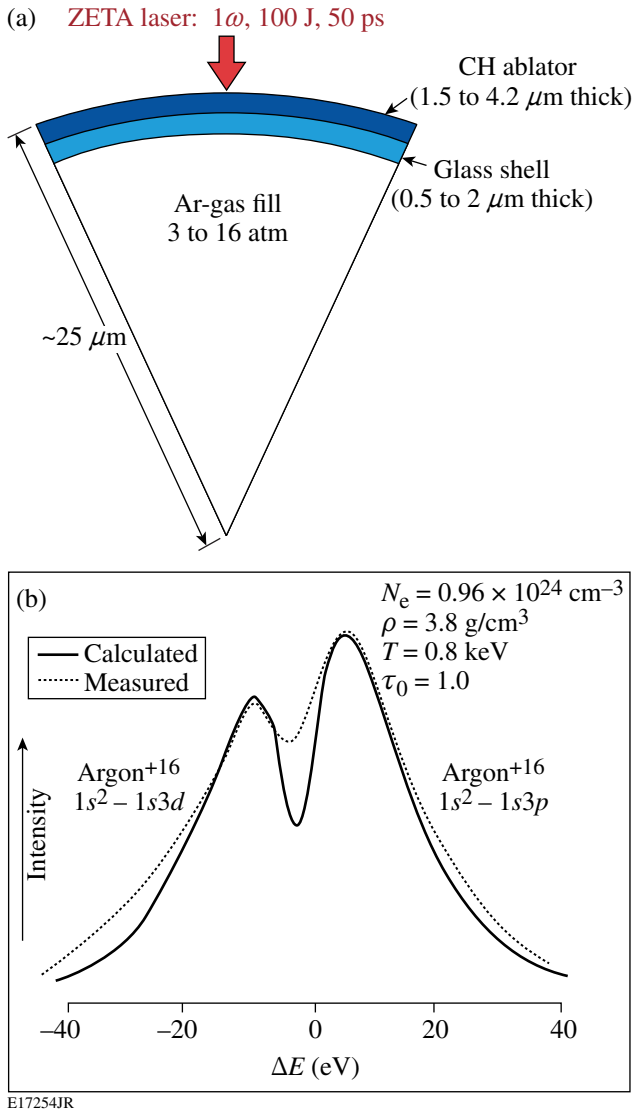

Figure 118.5
(a) Schematic of a direct-drive target, consisting of a thin glass shell with a plastic ablator filled with Ar gas, used in implosion compression experiments on the ZETA Laser System. (b) Measured, time-integrated x-ray spectrum of the Stark-broadened Ar He_β emission (dotted curve) compared to the predicted[30] spectral line shape (solid curve).

tral Laser Facility by self-consistently fitting all the observed lines of one state of ionization to diagnose electron density and opacity.[49] Hooper *et al.* used an x-ray streak camera to record time-resolved Stark-broadened Ar K-shell emission from direct-drive implosions on OMEGA.[50] Hammel *et al.* used Stark-broadened Ar K-shell emission to study indirect-drive implosions on Nova.[51] Nishimura *et al.* used similar x-ray spectroscopic techniques to study indirect-drive implosions on the GEKKO XII Laser System.[52] Keane *et al.* extended the research on Nova with indirect-drive implosions using Xe L-shell emission.[53] Woolsey *et al.* inferred the temporal evolution of electron temperature and density in indirectly driven spherical implosions on Nova.[54] Haynes *et al.* studied the effects of ion dynamics and opacity on Stark-broadened Ar K-shell emission on OMEGA.[34]

State-of-the-art measurements using Stark-broadened K-shell emission from implosion cores were performed on OMEGA.[13] As shown in Fig. 118.6(a), a plastic-shell target (20 μm thick and 860 μm in diameter) with an Ar-doped deu-

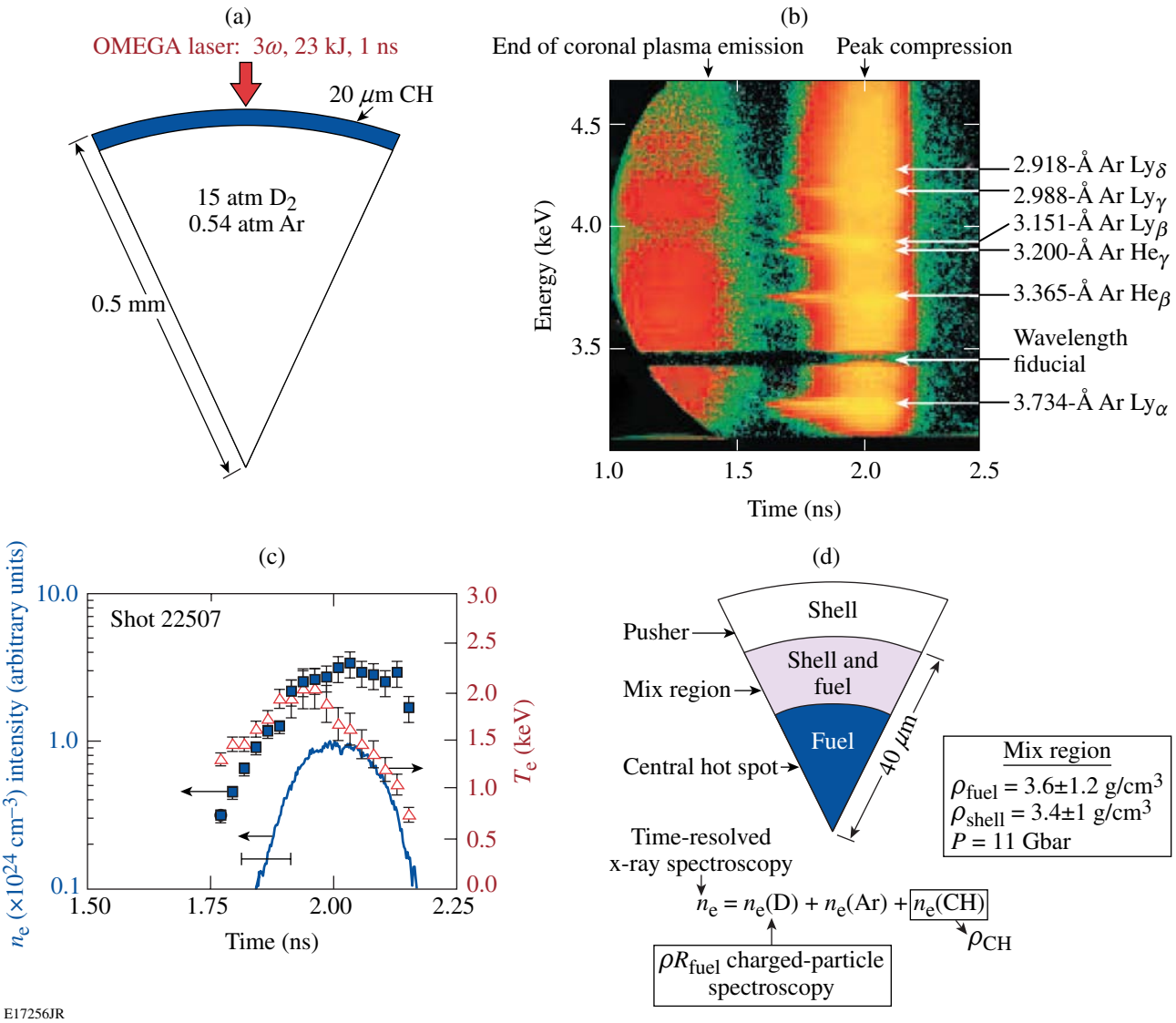

Figure 118.6

(a) Schematic of a direct-drive target, consisting of a 20-μm-thick plastic shell filled with deuterium gas doped with Ar, used in implosion compression experiments on the 60-beam OMEGA Laser System. (b) Measured, time-resolved Stark-broadened Ar K-shell emission. (c) Emissivity-averaged electron temperature (triangles) and density (squares) inferred from time-resolved Ar K-shell x-ray spectroscopy and ~3.5-keV x-ray continuum (solid curve) emitted from the implosion. (d) Schematic of the physical picture of the compressed core at peak neutron production showing an RT-induced mix region, consisting of shell and fuel, formed between the shell and the fuel.

terium fill gas was driven with a 23-kJ, 1-ns square laser pulse smoothed with phase plates,[25] 2-D SSD,[26] and PS.[27] Compared to the targets used for the seminal work on ZETA,[12] the gas-filled spherical-shell implosion targets on OMEGA were more than an order of magnitude larger than previously used. The time-resolved Ar K-shell emission dispersed with a Bragg crystal and recorded with an x-ray streak camera is shown in Fig. 118.6(b), with the prominent spectral features identified. The spectral line shapes were analyzed with the MERL code[32] to infer the time history of the emissivity-averaged electron temperature and density in the implosion core shown in Fig. 118.6(c). This diagnostic technique charts the evolution of the implosion dynamics. A strong rise in the electron temperature and density is observed as the shell decelerates. The peak in the electron temperature occurs at peak neutron production time, and peak compression occurs at stagnation when peak x-ray production is observed. The RT-induced fuel–shell mix in implosions was estimated[40] by combining the density inferred from Ar K-shell spectroscopy[13] and the areal density inferred from charged-particle spectroscopy.[41] The physical picture of the compressed core is shown schematically in Fig. 118.6(d). A mix region consisting of plastic shell and Ar-doped deuterium gas develops between the shell pusher and the fuel in the central hot spot. The electron density in the mix region is inferred from the Ar K-shell spectroscopy.[12,40] The deuterium fuel, Ar dopant, and any plastic shell material contribute to the electron density in the mix region. The contribution from the deuterium fuel was estimated from the fuel-areal-density measurement,[41] and the contribution from Ar was calculated to be small. A ratio of approximately 1:1 of plastic and fuel in the mix region was inferred.[40]

3. X-Ray Absorption Spectroscopy

Many of the high-energy-density plasmas created during the implosion are too cold to emit x rays. X-ray absorption spectroscopy effectively characterizes such matter. The relatively cold conditions in the imploding shell (the "piston") were first diagnosed by Yaakobi using x-ray absorption spectroscopy.[14] The four-beam, 1ω, 0.2-TW, 60- to 70-ps DELTA Laser System irradiated thin (~1-μm-thick) spherical glass shells or thick (~8-μm-thick) spherical plastic-coated glass shells, 60 to 110 μm in diameter and filled with either 7 to 20 atm of Ar gas or 18 atm of DT, as shown in Fig. 118.7(a). Figure 118.7(b) shows the time-integrated x-ray absorption spectra for two shots.[14] Both spectra show prominent Si K-shell emissions from the inner wall of the shell that is heated by heat conduction from the hot spot and by the shock wave reflected from the center of the target. The outgoing x-ray continuum emission from the hot spot and the inner wall of the imploding shell backlights the compressed shell. The lower spectrum in Fig. 118.7(b) showing Si 1s–2p absorption features from B-like Si (i.e., Si^{9+}) to He-like Si (i.e., Si^{12+}) ions indicates that a relatively cold (i.e.,

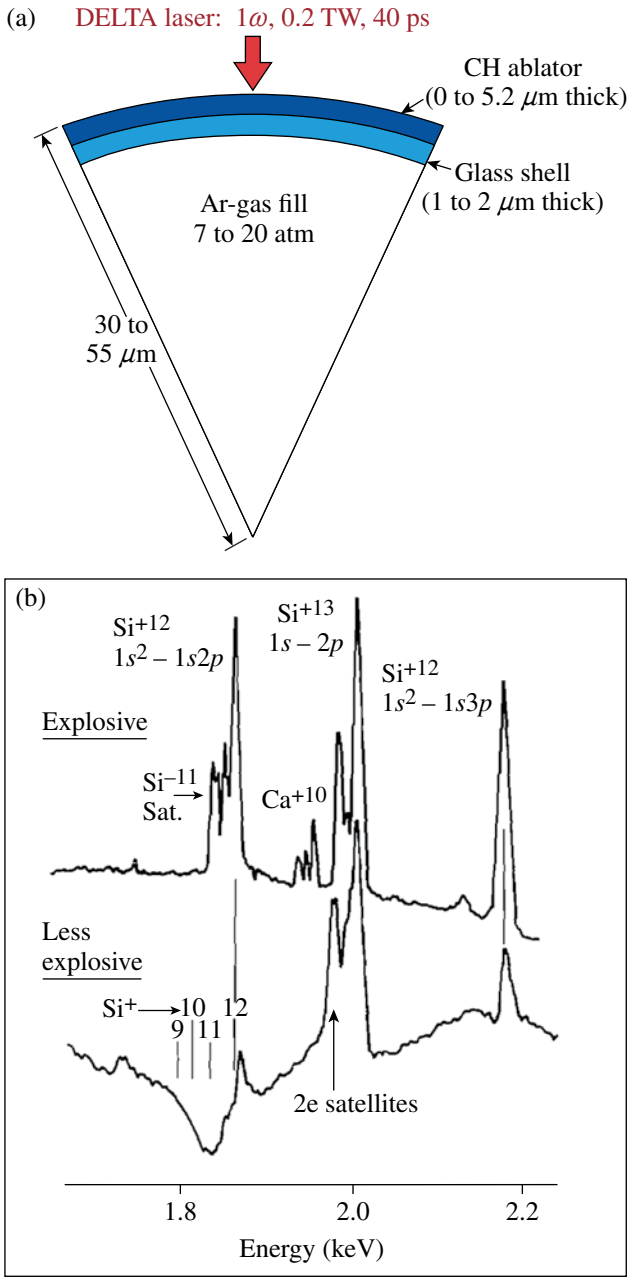

E17257JR

Figure 118.7
(a) Schematic of a direct-drive target, consisting of a thin glass shell with a plastic ablator filled with Ar gas, used in x-ray absorption spectroscopy experiments on the DELTA Laser System. (b) Measured, time-integrated x-ray spectrum of the Si K-shell spectrum taken for an explosive pusher (upper spectrum) and an ablatively driven implosion (lower trace). The Si 1s–2p absorption is observed in the latter case.

$T_e < 200$ eV) dense shell surrounds the hot spot,[14] which is characteristic of an ablatively driven implosion.[3,4] The absence of Si 1*s*–2*p* absorption features in the upper trace of Fig. 118.7(b) indicates that the glass shell material surrounding the hot spot is not cold (i.e., $T_e > 200$ eV); rather it is characteristic of an exploding pusher implosion.

Applications of x-ray absorption spectroscopy are not limited to compressed matter. Novel point-projection x-ray absorption spectroscopy experiments were performed using indirect drive[55] on Nova. X-ray–heated samples of Al were diagnosed using Al 1*s*–2*p* spectroscopy.[55]

State-of-the-art measurements using x-ray absorption spectroscopy have been performed on OMEGA to diagnose the shock-heated and compressed matter characteristic of the shock-propagation stage.[15,16] These results greatly benefit from earlier work by Hoarty *et al.*,[56] Boehly *et al.*,[57] and A. Ng.[58] As shown in Fig. 118.8(a), plastic planar-foil targets (50 μm thick) with a buried layer of Al (~1 μm thick) were shock heated and compressed by directly irradiating planar targets with high-intensity laser beams, generating 10- to 70-Mbar shock-wave pressures with on-target intensities in the range of 0.05 to 1.0×10^{15} W/cm^2 over a 0.5-mm diameter.[15] The buried depth was varied to probe the shock wave at different

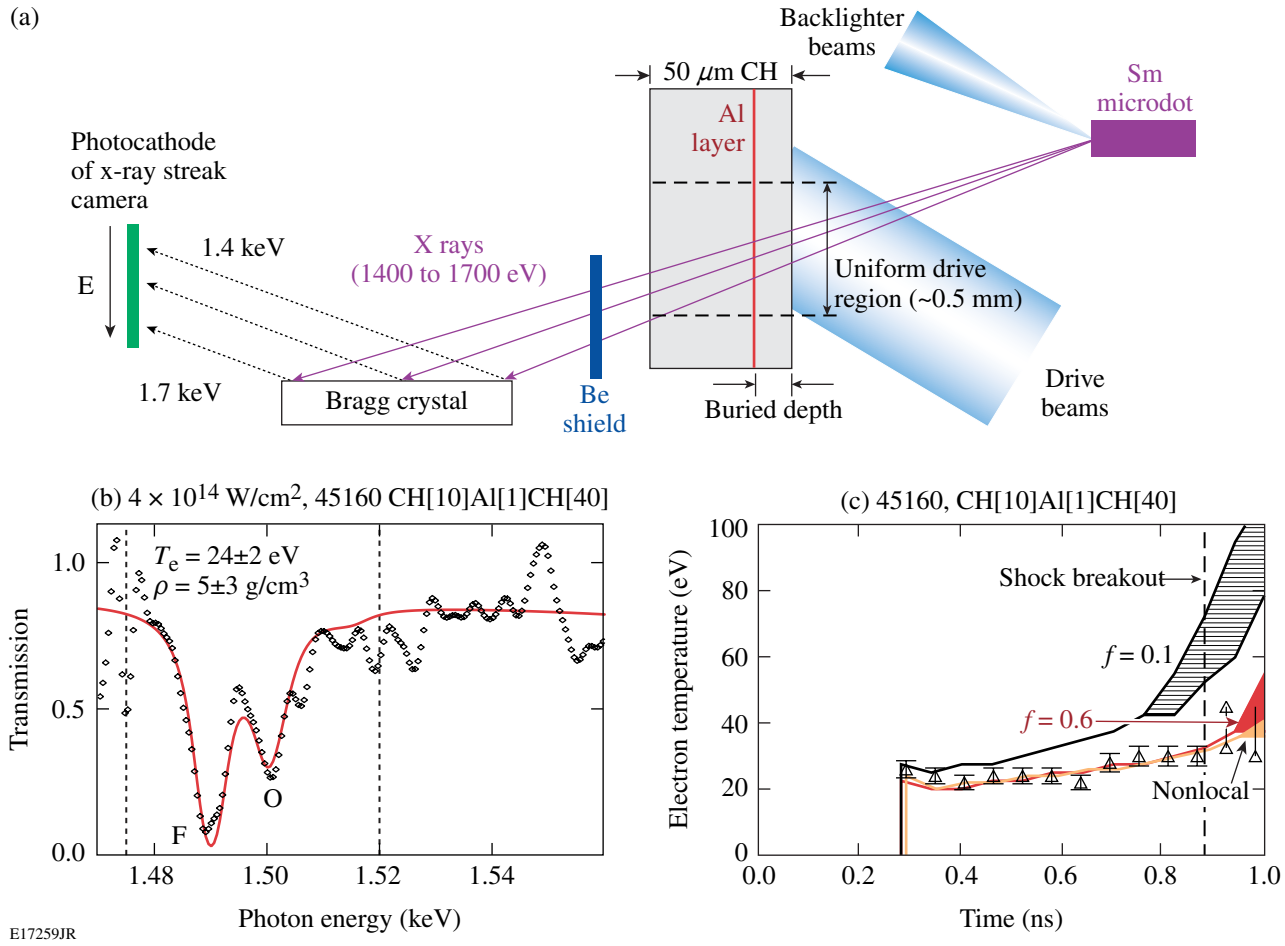

Figure 118.8
(a) Schematic of an experimental setup for a time-resolved x-ray absorption spectroscopy experiment on the 60-beam OMEGA laser to diagnose laser-ablation–driven shock heating and compression. (b) Time-resolved Al 1*s*–2*p* absorption spectrum recorded after the shock wave propagated through the buried Al layer. (c) Time history of the electron temperature in the Al layer compared with various 1-D hydrodynamic models. The shock wave passes through the buried Al layer just after 0.2 ns and breaks out of the rear surface of the target just after 0.8 ns.

times. The shock wave creates nearly uniform conditions in the Al layer. A separate group of tightly focused beams with an intensity of ~10^{16} W/cm^2 irradiated the Sm point-source (100-μm-diam) backlighter producing a pseudo-continuum of Sm M-shell emission in the 1400- to 1700-eV photon energy range.[15] The resulting warm dense matter was probed with time-resolved Al 1s–2p absorption spectroscopy, using a Bragg crystal spectrometer and an x-ray streak camera arranged as shown in Fig. 118.8(a), to infer temperature and density in the buried Al layer.[15] Al 1s–2p absorption provides the experimental signature of shock-wave ionization of the buried Al layer. The density is inferred from the Stark broadening of the spectral line shapes, and the temperature is inferred from the relative distribution of the various absorption charge states.[15,32,35] An Al 1s–2p absorption spectrum recorded after a single, strong laser-ablation–driven shock wave propagated through the buried Al layer is shown in Fig. 118.8(b). The drive intensity was 4×10^{14} W/cm^2. Prominent F-like and O-like Al 1s–2p features are observed.[15] Higher charge states of Al are ionized in succession and absorbed in 1s–2p transitions as the electron temperature increases. A time history of the inferred temperature in the buried Al layer is presented in Fig. 118.8(c) and compared with different models of electron thermal conduction.[15] The nonlocal model and the flux-limited model with $f = 0.06$ show good agreement with the experimental results for this drive condition.[15] Dense, Fermi-degenerate Al created using multiple shock waves was diagnosed with Al 1s–2p absorption spectroscopy to be compressed to 4× solid density (11±5 g/cm^3) and heated to 20±2 eV (Refs. 15 and 16).

4. Multispectral Monochromatic X-Ray Imaging

Azechi *et al.* obtained the first multiple monochromatic images of implosion cores by placing a pinhole array in front of a flat Bragg crystal.[17] Thin glass shells (1 μm thick and 60 μm in diameter) filled with 3.5 atm of Ne, as shown in Fig. 118.9(a), were imploded on the two-beam, 1ω, 45-J, 120-ps GEKKO II Laser System[5] and backlit with x rays to diagnose the temperature and areal density of the implosion core.[17] The experimental setup for the backlighting using multifrequency x rays (i.e., multiple monochromatic x-ray images) is shown in Fig. 118.9(b). The concept of combining a pinhole aperture with a Bragg crystal spectrometer to achieve multiple monochromatic x-ray images was extended to hundreds of pinholes nearly two decades later on OMEGA.[18] As shown in Fig. 118.10(a), a plastic shell target (28 μm thick and 920 μm in diameter) with an inner Ti-doped plastic layer and a 10-atm-deuterium-gas fill was driven with a 30-kJ, 1-ns square laser pulse. The time-integrated multiple monochromatic images recorded during the implosion are presented in Fig. 118.10(b), with the prominent Ti K-shell emission and Ti K_α emission identified.

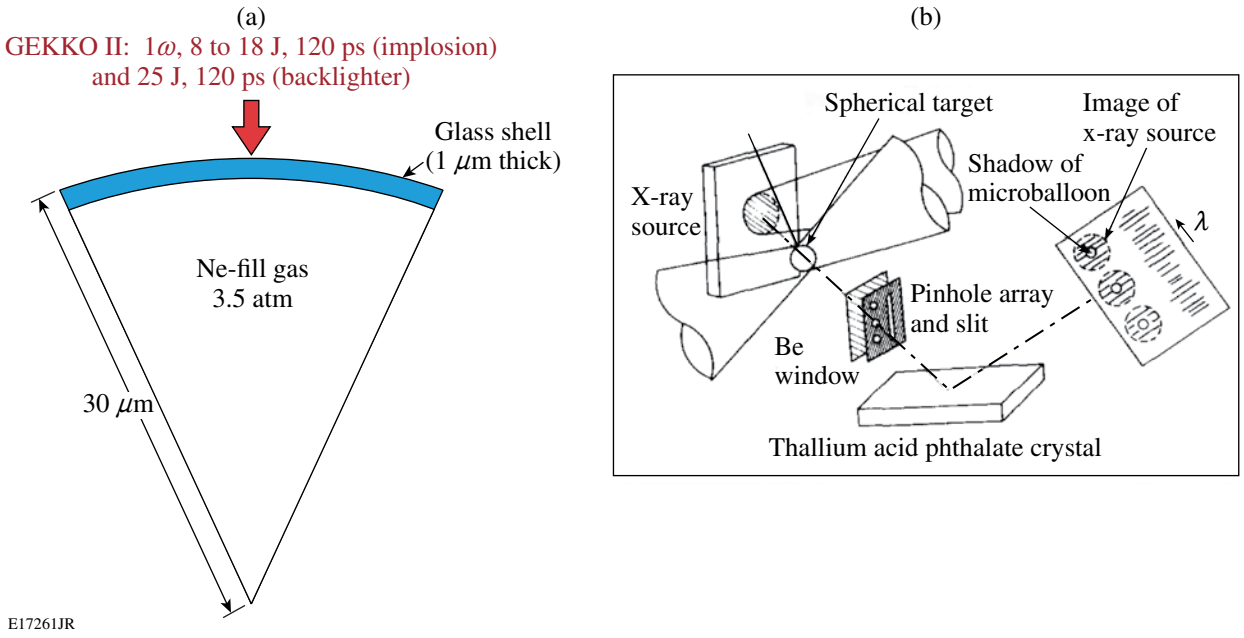

Figure 118.9
(a) Schematic of a direct-drive glass-shell-implosion target filled with Ne gas and used in multifrequency x-ray backlighting experiments on the GEKKO II Laser System. (b) Schematic of the experimental setup for multifrequency x-ray backlighting.

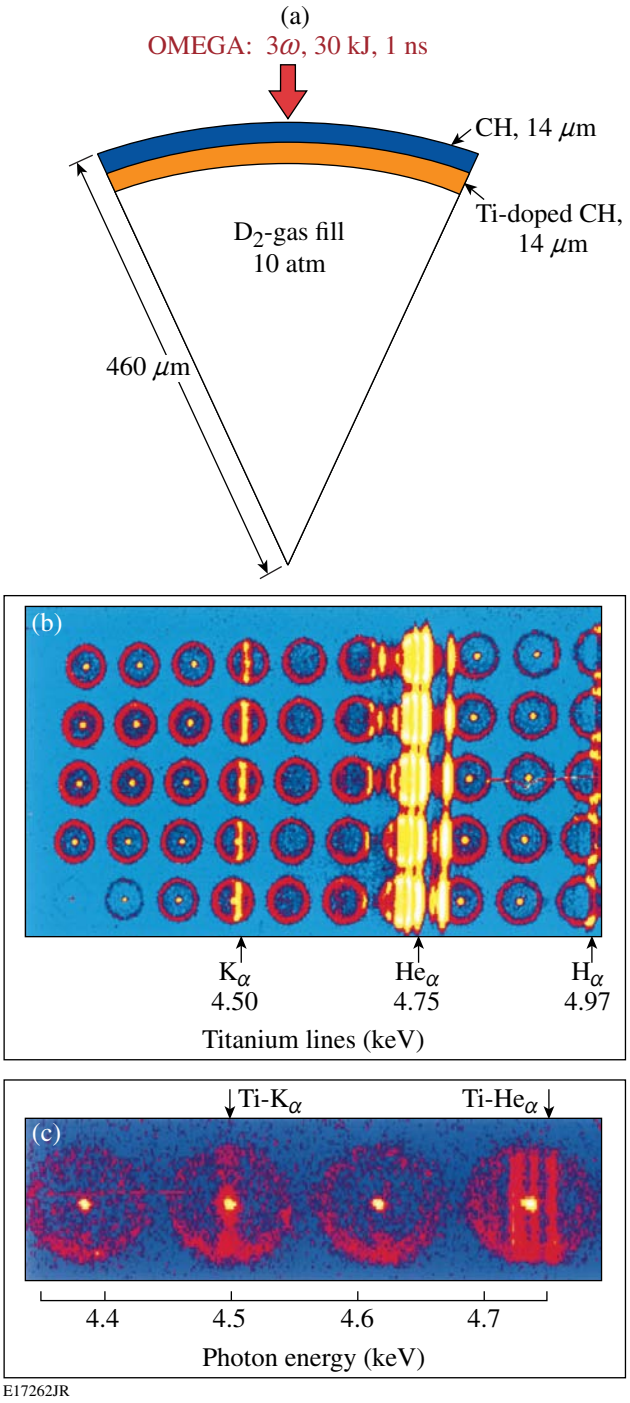

Figure 118.10
(a) Schematic of a direct-drive plastic-shell-implosion target used to demonstrate the pinhole-array x-ray spectrometer. The inner layer of the plastic shell is doped with trace amounts of Ti and the target is filled with deuterium gas. (b) A multiple monochromatic image recorded with a pinhole-array x-ray spectrometer with the prominent Ti K-shell emission identified. (c) Image highlighting the cold Ti-doped portion of the shell pumped by an x-ray continuum from the core emits Ti K_α emission.

The outermost ring of emission is from the coronal plasma and the bright central spot is emission from the hot spot. The cold Ti-doped portion of the shell pumped by an x-ray continuum from the core emits Ti K_α emission, as shown in Fig. 118.10(c). The vertical profile of the Ti K_α emission shows the true dimension of the cold shell at peak compression.[18]

Current state-of-the-art multiple monochromatic imaging involved synchronized, time-resolved images from multiple lines of sight for direct-drive implosions on OMEGA of Ar-doped-deuterium–filled plastic-shell targets recorded by Roberto Mancini's research group.[20] Multiple monochromatic images from three quasi-orthogonal lines of sight of the Ly_β emission profiles of a direct-drive implosion are shown in Fig. 118.11(a). Koch *et al*. designed a multiple monochromatic imager for Ar K-shell emission from indirect-drive-implosion cores.[59] Welser-Sherrill *et al*. used the images of the Ar K-shell emission lines to diagnose electron density and temperature spatial profiles in the cores of indirect-drive implosions.[19] Tommasini redesigned a multiple monochromatic imager for Ar K-shell emission for direct-drive-implosion cores,[60] which have better diagnostic access, simpler targets, and higher electron temperatures in the implosion core than indirect-drive implosions on OMEGA. The multiple monochromatic imaging using multiple lines of sight [see Fig. 118.11(a)] for the He_β and Ly_β emission profiles were used to infer the electron-temperature profile of the direct-drive-implosion core shown in Fig. 118.11(b).[61]

Conclusions

X-ray spectroscopy has been used to chart the remarkable progress of laser-fusion experiments over the last three decades. Hans Griem provided the foundation for this research. He studied the effect of plasma particles, in particular the fast-moving free electrons, on the Stark-broadening of spectral line shapes in plasmas. Four areas of x-ray spectroscopy for laser-fusion experiments were highlighted: K_α emission spectroscopy to diagnose target preheat by suprathermal electrons, Stark-broadened K-shell emissions of mid-Z elements to diagnose compressed densities and temperatures of implosion cores, K- and L-shell absorption spectroscopy to diagnose the relatively cold imploding shell that does not emit x rays, and multispectral monochromatic imaging of implosions to diagnose core temperature and density profiles. The seminal research leading to the original x-ray-spectroscopy experiments in these areas was discussed and compared to current state-of-the-art measurements.

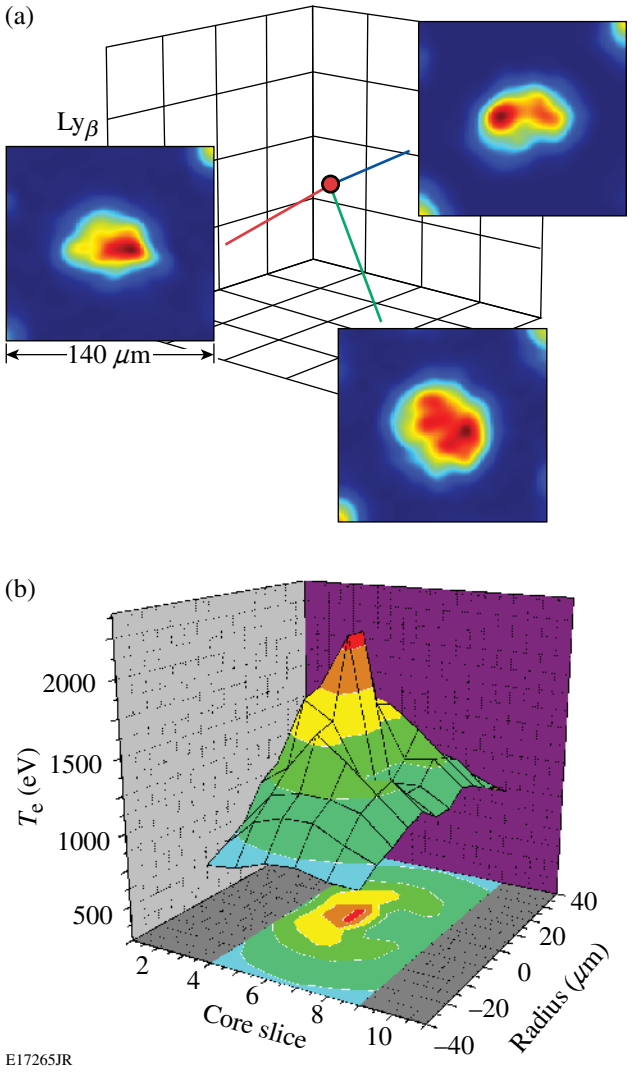

Figure 118.11
(a) Schematic of an experimental setup for time-resolved multiple monochromatic imaging of a direct-drive implosion in Ar Ly$_\beta$ emission performed along three quasi-orthogonal views. (b) Temperature profile inferred from analyzing time-resolved multiple monochromatic imaging of a direct-drive implosion in Ar Ly$_\beta$ and He$_\beta$ emissions performed along three quasi-orthogonal views.

ACKNOWLEDGMENT

This work was supported by the U.S. Department of Energy Office of Inertial Confinement Fusion under Cooperative Agreement No. DE-FC52-08NA28302, the University of Rochester, and the New York State Energy Research and Development Authority. The support of DOE does not constitute an endorsement by DOE of the views expressed in this article.

REFERENCES

1. H. R. Griem, *Principles of Plasma Spectroscopy* (Cambridge University Press, Cambridge, England, 1997).
2. R. L. McCrory, D. D. Meyerhofer, R. Betti, R. S. Craxton, J. A. Delettrez, D. H. Edgell, V. Yu Glebov, V. N. Goncharov, D. R. Harding, D. W. Jacobs-Perkins, J. P. Knauer, F. J. Marshall, P. W. McKenty, P. B. Radha, S. P. Regan, T. C. Sangster, W. Seka, R. W. Short, S. Skupsky, V. A. Smalyuk, J. M. Soures, C. Stoeckl, B. Yaakobi, D. Shvarts, J. A. Frenje, C. K. Li, R. D. Petrasso, and F. H. Séguin, Phys. Plasmas **15**, 055503 (2008); P. W. McKenty, V. N. Goncharov, R. P. J. Town, S. Skupsky, R. Betti, and R. L. McCrory, Phys. Plasmas **8**, 2315 (2001).
3. J. D. Lindl, *Inertial Confinement Fusion: The Quest for Ignition and Energy Gain Using Indirect Drive* (Springer-Verlag, New York, 1998); J. D. Lindl *et al.*, Phys. Plasmas **11**, 339 (2004).
4. E. Snitzer, Phys. Rev. Lett. **7**, 444 (1961).
5. G. Verlarde and N. Carpintero–Santamaría, *Inertial Confinement Nuclear Fusion: A Historical Approach by Its Pioneers* [Foxwell & Davies (UK) Ltd., London, 2007].
6. B. Yaakobi, I. Pelah, and J. Hoose, Phys. Rev. Lett. **37**, 836 (1976).
7. J. D. Hares *et al.*, Phys. Rev. Lett. **42**, 1216 (1979).
8. B. Yaakobi, C. Stoeckl, T. Boehly, D. D. Meyerhofer, and W. Seka, Phys. Plasmas **7**, 3714 (2000).
9. B. Yaakobi, C. Stoeckl, W. Seka, J. A. Delettrez, T. C. Sangster, and D. D. Meyerhofer, Phys. Plasmas **12**, 062703 (2005); V. A. Smalyuk, D. Shvarts, R. Betti, J. A. Delettrez, D. H. Edgell, V. Yu. Glebov, V. N. Goncharov, R. L. McCrory, D. D. Meyerhofer, P. B. Radha, S. P. Regan, T. C. Sangster, W. Seka, S. Skupsky, C. Stoeckl, B. Yaakobi, J. A. Frenje, C. K. Li, R. D. Petrasso, and F. H. Séguin, Phys. Rev. Lett. **100**, 185005 (2008).
10. K. Yasuike *et al.*, Rev. Sci. Instrum. **72**, 1236 (2001).
11. B. Yaakobi, D. Steel, E. Thorsos, A. Hauer, and B. Perry, Phys. Rev. Lett. **39**, 1526 (1977).
12. B. Yaakobi, S. Skupsky, R. L. McCrory, C. F. Hooper, H. Deckman, P. Bourke, and J. M. Soures, Phys. Rev. Lett. **44**, 1072 (1980).
13. S. P. Regan, J. A. Delettrez, R. Epstein, P. A. Jaanimagi, B. Yaakobi, V. A. Smalyuk, F. J. Marshall, D. D. Meyerhofer, W. Seka, D. A. Haynes Jr., I. E. Golovkin, and C. F. Hooper Jr., Phys. Plasmas **9**, 1357 (2002).
14. B. Yaakobi, R. L. McCrory, S. Skupsky, J. A. Delettrez, P. Bourke, H. Deckman, C. F. Hooper, and J. M. Soures, Opt. Commun. **34**, 213 (1980).
15. H. Sawada, S. P. Regan, P. B. Radha, R. Epstein, D. Li, V. N. Goncharov, S. X. Hu, D. D. Meyerhofer, J. A. Delettrez, P. A. Jaanimagi, V. A. Smalyuk, T. R. Boehly, T. C. Sangster, B. Yaakobi, and R. C. Mancini, Phys. Plasmas **16**, 052702 (2009).

16. S. P. Regan, H. Sawada, V. N. Goncharov, D. Li, P. B. Radha, R. Epstein, J. A. Delettrez, S. X. Hu, V. A. Smalyuk, B. Yaakobi, T. C. Sangster, D. D. Meyerhofer, R. L. McCrory, and R. C. Mancini, "Spectroscopic Observations of Fermi-Degenerate Aluminum Compressed and Heated to Four Times Solid Density and 20 eV," submitted to Physical Review E.

17. H. Azechi *et al*., Appl. Phys. Lett. **37**, 998 (1980).

18. B. Yaakobi, F. J. Marshall, and D. K. Bradley, Appl. Opt. **37**, 8074 (1998).

19. L. Welser-Sherrill, R. C. Mancini, J. A. Koch, N. Izumi, R. Tommasini, S. W. Haan, D. A. Haynes, I. E. Golovkin, J. J. MacFarlane, J. A. Delettrez, F. J. Marshall, S. P. Regan, V. A. Smalyuk, and G. Kyrala, Phys. Rev. E **76**, 056403 (2007).

20. L. A. Welser, R. C. Mancini, J. A. Koch, N. Izumi, H. Dalhed, H. Scott, T. W. Barbee Jr., R. W. Lee, I. E. Golovkin, F. Marshall, J. Delettrez, and L. Klein, J. Quant. Spectrosc. Radiat. Transf. **81**, 487 (2003).

21. J. Soures, L. M. Goldman, and M. Lubin, Nucl. Fusion **13**, 829 (1973).

22. T. R. Boehly, D. L. Brown, R. S. Craxton, R. L. Keck, J. P. Knauer, J. H. Kelly, T. J. Kessler, S. A. Kumpan, S. J. Loucks, S. A. Letzring, F. J. Marshall, R. L. McCrory, S. F. B. Morse, W. Seka, J. M. Soures, and C. P. Verdon, Opt. Commun. **133**, 495 (1997).

23. L. J. Waxer, D. N. Maywar, J. H. Kelly, T. J. Kessler, B. E. Kruschwitz, S. J. Loucks, R. L. McCrory, D. D. Meyerhofer, S. F. B. Morse, C. Stoeckl, and J. D. Zuegel, Opt. Photonics News **16**, 30 (2005); C. Stoeckl, J. A. Delettrez, J. H. Kelly, T. J. Kessler, B. E. Kruschwitz, S. J. Loucks, R. L. McCrory, D. D. Meyerhofer, D. N. Maywar, S. F. B. Morse, J. Myatt, A. L. Rigatti, L. J. Waxer, J. D. Zuegel, and R. B. Stephens, Fusion Sci. Technol. **49**, 367 (2006).

24. S. P. Regan, J. A. Marozas, R. S. Craxton, J. H. Kelly, W. R. Donaldson, P. A. Jaanimagi, D. Jacobs-Perkins, R. L. Keck, T. J. Kessler, D. D. Meyerhofer, T. C. Sangster, W. Seka, V. A. Smalyuk, S. Skupsky, and J. D. Zuegel, J. Opt. Soc. Am. B **22**, 998 (2005).

25. T. J. Kessler, Y. Lin, J. J. Armstrong, and B. Velazquez, in *Laser Coherence Control: Technology and Applications*, edited by H. T. Powell and T. J. Kessler (SPIE, Bellingham, WA, 1993), Vol. 1870, pp. 95–104; Y. Lin, T. J. Kessler, and G. N. Lawrence, Opt. Lett. **21**, 1703 (1996).

26. S. Skupsky, R. W. Short, T. Kessler, R. S. Craxton, S. Letzring, and J. M. Soures, J. Appl. Phys. **66**, 3456 (1989); S. Skupsky and R. S. Craxton, Phys. Plasmas **6**, 2157 (1999).

27. Y. Kato, unpublished notes from work at LLE, 1984; K. Tsubakimoto *et al*., Opt. Commun. **103**, 185 (1993); *LLE Review Quarterly Report* **71**, 145, Laboratory for Laser Energetics, University of Rochester, Rochester, NY, LLE Document No. DOE/SF/19460-186, NTIS Order No. DE98000308 (1997); T. E. Gunderman, J.-C. Lee, T. J. Kessler, S. D. Jacobs, D. J. Smith, and S. Skupsky, in *Conference on Lasers and Electro-Optics*, Vol. 7, 1990 OSA Technical Digest Series (Optical Society of America, Washington, DC, 1990), p. 354; T. R. Boehly, V. A. Smalyuk, D. D. Meyerhofer, J. P. Knauer, D. K. Bradley, R. S. Craxton, M. J. Guardalben, S. Skupsky, and T. J. Kessler, J. Appl. Phys. **85**, 3444 (1999).

28. R. L McCrory and R. L. Morse, Phys. Rev. Lett. **38**, 544 (1977); R. S. Craxton, Opt. Commun. **34**, 474 (1980); R. S. Craxton, S. D. Jacobs, J. E. Rizzo, and R. Boni, IEEE J. Quantum Electron. **QE-17**, 1782 (1981); W. Seka, S. D. Jacobs, J. E. Rizzo, R. Boni, and R. S. Craxton, Opt. Commun. **34**, 469 (1980).

29. B. L. Henke and P. A. Jaanimagi, Rev. Sci. Instrum. **56**, 1537 (1985).

30. R. J. Tighe and C. F. Hooper Jr., Phys. Rev. A **14**, 1514 (1976).

31. R. F. Joyce, L. A. Woltz, and C. F. Hooper Jr., Phys. Rev. A **35**, 2228 (1987).

32. R. C. Mancini *et al*., Comput. Phys. Commun. **63**, 314 (1991).

33. C. A. Iglesias, J. L. Lebowitz, and D. MacGowan, Phys. Rev. A **28**, 1667 (1983).

34. D. A. Haynes Jr., D. T. Garber, C. F. Hooper Jr., R. C. Mancini, Y. T. Lee, D. K. Bradley, J. Delettrez, R. Epstein, and P. A. Jaanimagi, Phys. Rev. E **53**, 1042 (1996).

35. J. J. MacFarlane *et al*., High Energy Density Phys. **3**, 181 (2006).

36. G. E. Moore, Electronics **38**, 114 (1965).

37. J. A. Paisner, E. M. Campbell, and W. J. Hogan, Fusion Technol. **26**, 755 (1994); G. H. Miller, E. I. Moses, and C. R. Wuest, Opt. Eng. **43**, 2841 (2004).

38. D. W. Phillion *et al*., Phys. Rev. Lett. **49**, 1405 (1982); D. M. Villeneuve, R. L. Keck, B. B. Afeyan, W. Seka, and E. A. Williams, Phys. Fluids **27**, 721 (1984); C. Rousseaux *et al*., Phys. Fluids B **4**, 2589 (1992); W. Seka, R. E. Bahr, R. W. Short, A. Simon, R. S. Craxton, D. S. Montgomery, and A. E. Rubenchik, Phys. Fluids B **4**, 2232 (1992); C. S. Liu and M. N. Rosenbluth, Phys. Fluids **19**, 967 (1976); A. Simon, R. W. Short, E. A. Williams, and T. Dewandre, Phys. Fluids **26**, 3107 (1983); A. B. Langdon, B. F. Lasinski, and W. L. Kruer, Phys. Rev. Lett. **43**, 133 (1979); B. F. Lasinski and A. B. Langdon, Lawrence Livermore National Laboratory, Livermore, CA, Report UCRL-50021-77, 4-49 (1978); B. B. Afeyan and E. A. Williams, Phys. Plasmas **4**, 3827 (1997); C. Stoeckl, R. E. Bahr, B. Yaakobi, W. Seka, S. P. Regan, R. S. Craxton, J. A. Delettrez, R. W. Short, J. Myatt, A. V. Maximov, and H. Baldis, Phys. Rev. Lett. **90**, 235002 (2003).

39. W. L. Kruer, *The Physics of Laser–Plasma Interactions*, Frontiers in Physics, Vol. 73, edited by D. Pines (Addison-Wesley, Redwood City, CA, 1988), Chap. 4, pp. 37–43.

40. S. P. Regan, J. A. Delettrez, F. J. Marshall, J. M. Soures, V. A. Smalyuk, B. Yaakobi, V. Yu. Glebov, P. A. Jaanimagi, D. D. Meyerhofer, P. B. Radha, W. Seka, S. Skupsky, C. Stoeckl, R. P. J. Town, D. A. Haynes Jr., I. E. Golovkin, C. F. Hooper Jr., J. A. Frenje, C. K. Li, R. D. Petrasso, and F. H. Séguin, Phys. Rev. Lett. **89**, 085003 (2002).

41. C. K. Li, F. H. Séguin, D. G. Hicks, J. A. Frenje, K. M. Green, S. Kurebayashi, R. D. Petrasso, D. D. Meyerhofer, J. M. Soures, V. Yu. Glebov, R. L. Keck, P. B. Radha, S. Roberts, W. Seka, S. Skupsky, C. Stoeckl, and T. C. Sangster, Phys. Plasmas **8**, 4902 (2001).

42. C. D. Zhou and R. Betti, Phys. Plasmas **15**, 102707 (2008).

43. M. C. Herrmann, M. Tabak, and J. D. Lindl, Nucl. Fusion **41**, 99 (2001).

44. R. Betti, K. Anderson, V. N. Goncharov, R. L. McCrory, D. D. Meyerhofer, S. Skupsky, and R. P. J. Town, Phys. Plasmas **9**, 2277 (2002).

45. M. Tabak and D. Callahan-Miller, Phys. Plasmas **5**, 1895 (1998); S. Atzeni, Phys. Plasmas **6**, 3316 (1999); M. H. Key, Phys. Plasmas **14**, 055502 (2007).

46. M. D. Rosen and J. H. Nuckolls, Phys. Fluids **22**, 1393 (1979).

47. C. Stoeckl, V. Yu. Glebov, D. D. Meyerhofer, W. Seka, B. Yaakobi, R. P. J. Town, and J. D. Zuegel, Rev. Sci. Instrum. **72**, 1197 (2001).

48. J. M. Soures, T. C. Bristow, H. Deckman, J. Delettrez, A. Entenberg, W. Friedman, J. Forsyth, Y. Gazit, G. Halpern, F. Kalk, S. Letzring, R. McCrory, D. Peiffer, J. Rizzo, W. Seka, S. Skupsky, E. Thorsos, B. Yaakobi, and T. Yamanaka, in *Laser Interaction and Related Plasma Phenomena*, edited by H. J. Schwarz, H. Hora, M. J. Lubin, and B. Yaakobi (Plenum Press, New York, 1981), Vol. 5, pp. 463–481.

49. J. D. Kilkenny *et al*., Phys. Rev. A **22**, 2746 (1980).

50. C. F. Hooper Jr., D. P. Kilcrease, R. C. Mancini, L. A. Woltz, D. K. Bradley, P. A. Jaanimagi, and M. C. Richardson, Phys. Rev. Lett. **63**, 267 (1989).

51. B. A. Hammel *et al*., Phys. Rev. Lett. **70**, 1263 (1993).

52. H. Nishimura *et al*., Phys. Plasmas **2**, 2063 (1995).

53. C. J. Keane *et al*., Phys. Rev. Lett. **72**, 3029 (1994).

54. N. C. Woolsey *et al*., Phys. Rev. E **56**, 2314 (1997).

55. T. S. Perry *et al*., Phys. Rev. Lett. **67**, 3784 (1991).

56. D. Hoarty *et al*., Phys. Rev. Lett. **78**, 3322 (1997).

57. T. R. Boehly, J. A. Delettrez, J. P. Knauer, D. D. Meyerhofer, B. Yaakobi, R. P. J. Town, and D. Hoarty, Phys. Rev. Lett. **87**, 145003 (2001).

58. A. Ng, Lawrence Livermore National Laboratory, private communication (2006).

59. J. A. Koch, T. W. Barbee Jr., N. Izumi, R. Tommasini, R. C. Mancini, L. A. Welser, and F. J. Marshall, Rev. Sci. Instrum. **76**, 073708 (2005).

60. R. Tommasini, J. A. Koch, N. Izumi, L. A. Welser, R. C. Mancini, J. Delettrez, S. Regan, and V. Smalyuk, Rev. Sci. Instrum. **77**, 10E303 (2006).

61. T. Nagayama, R. C. Mancini, R. Florido, R. Tommasini, J. A. Koch, J. A. Delettrez, S. P. Regan, V. A. Smalyuk, L. A. Welser-Sherrill, and I. E. Golovkin, Rev. Sci. Instrum. **79**, 10E921 (2008).